Selective Release of Multiple DNA Oligonucleotides from Gold Nanorods

Selective Release of Multiple DNA Oligonucleotides from Gold Nanorods

Andy Wijaya[1], Stefan B. Schaffer[2], Ivan G. Pallares[3], and Kimberly Hamad-Schifferli[4,5,]*

[1]Department of Chemical Engineering, Massachusetts Institute of Technology, 77 Massachusetts Ave, Cambridge, MA 02139, [2]Division of Biology and Medicine, Brown University, Providence, RI 02912, [3] Department of Chemistry, University of North Carolina at Chapel Hill, Chapel Hill, NC 27599-3475, Departments of [4]Biological Engineering and [5]Mechanical Engineering, Massachusetts Institute of Technology, 77 Massachusetts Ave, Cambridge, MA 02139

*Corresponding author. Email: schiffer@mit.edu

RECEIVED DATE

CORRESPONDING AUTHOR FOOTNOTE

ABSTRACT

Combination therapy, or the use of multiple drugs, has been proven to be effective for complex diseases, but the differences in chemical properties and pharmacokinetics can be challenging in term of the loading, delivering, and releasing multiple drugs. Here we demonstrate that we can load and selectively release two different DNA oligonucleotides from two different gold nanorods. DNA was loaded on the nanorods via thiol conjugation. Selective releases were induced by selective melting of gold nanorods via ultrafast laser irradiation at the nanorods' longitudinal surface plasmon resonance peaks. Excitation at one wavelength could selectively melt one type of gold nanorods and selectively release one type

DNA strand. Releases were efficient (50-80%) and externally tunable by laser fluence. Released oligonucleotides were still functional. This proof of concept is potentially a powerful method for multiple-drug delivery strategies.

KEYWORDS (5-7 Keywords). gold nanorods, DNA oligonucleotide, drug delivery, controlled release, selective, independent control, combination therapy.

MANUSCRIPT TEXT

Increasingly, the use of multiple drugs, known as combination therapy, has been sought for improving treatment efficacy of diseases such as malaria,[1] cancer,[2] and HIV.[3] Though proven to be effective, the differences in the chemical properties (such as molecular weights, solubilities) and pharmacokinetics of the components of a drug mixture can create challenges for loading, delivery, and release of multiple durgs.[4] Even if a pre-determined synergistic ratio is encapsulated in a carrier, this ratio may not be maintained at a target upon delivery or during release. Typically, the timing of the release of each species is crucial for drug efficacy, as has been observed for tumor treatment.[2] Therefore, for effective combination therapy, release rates of each drug must be controlled independently. Current solutions involve complex systems such as polymer multilayers[5] or sophisticated bioMEMS implants.[6, 7] Nanoscale carriers have gained attraction, but achieving different release windows for each drug in a mixture requires engineering intricate architectures.[2] Extending all of these strategies beyond two species or even changing the order of release is problematical. Clearly, an effective method to externally control release of each species independently and actively would ultimately lead to optimization of combination therapies for treatment.

Recently, gold, [8, 9] magnetic,[10, 11] and composite[12] nanoparticles have been exploited for both passive and active targeted delivery.[13, 14] In the case of gold nanoparticles, the surface chemistry has been proven to be chemically versatile for loading biomolecules and optimizing physicochemical parameters.[9, 15] Gold nanorods (NRs) have also become attractive for biological applications due to their

optical properties.[16, 17] Pulsed laser excitation in resonance with their longitudinal surface plasmon resonance (SPR_{long}) can heat NRs locally to high temperatures,[18] inducing melting. This triggered melting is exploitable for controlling the release of biomolecules conjugated to the NRs.[19] Since SPR_{long} is tunable by changing NR aspect ratio (AR), NRs with different ARs can be excited independently at different wavelengths. If different NRs are conjugated to different molecules, this strategy could be utilized for orthogonal triggered release of multiple species. Others have utilized similar concept to independently control microfluidic valves using two different nanoparticles, gold colloids and gold nanoshells.[20]

Here we demonstrate selective release of two distinct DNA strands from two different NRs by matching laser excitation wavelength to the NRs' SPR_{long} (Scheme 1). We first demonstrate selective melting of two different NRs. Utilizing this concept, two different DNA oligonucleotides conjugated to each of the NRs were released selectively by irradiation at specific wavelengths, and released DNA was functional. The releases were also efficient (~50-80%) and externally controllable by tuning the laser fluence.

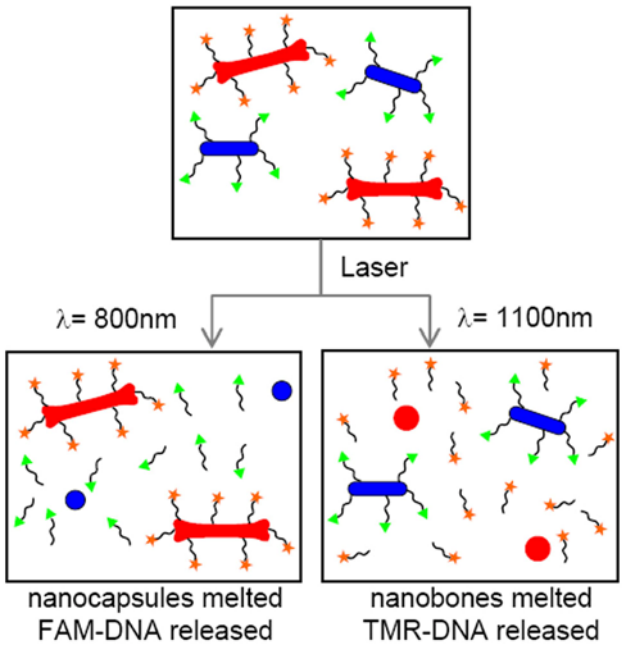

Scheme 1. Overview of selective release. Laser irradiation of DNA-conjugated nanocapsules (blue ovals) and nanobones (red bones) are exposed to λ_{800} irradiation (left), which melts the nanocapsules and selectively releases the conjugated DNA (labeled by FAM (green triangles)). Exposure to λ_{1100} irradiation (right) melts the nanobones, selectively releasing the conjugated DNA (labeled by TMR (orange stars)).

RESULTS AND DISCUSSION

NRs were synthesized[21-23] to have distinct ARs and morphologies, with SPR_{long} that overlapped with each of the laser excitation wavelengths. Short NRs, "nanocapsules," were ~11 nm × 44 nm, with <AR> = 4.0 (Fig. 1a, inset) and SPR_{long} at 800 nm (Fig. 1b, black), coinciding with the short wavelength excitation at ~800 nm (λ_{800}). Long NRs were bone-shaped (Fig. 2a, inset), presumably due to preferential deposition at the ends from the excess reducing agent.[21] "Nanobones" were ~17 × 89 nm with <AR> = 5.4 and SPR_{long} at ~1100 nm (Fig. 2b, black), coinciding with the long wavelength excitation at 1100 nm (λ_{1100}). Size analysis was done utilizing ImageJ.[24] Mixtures allowed distinction between their populations by both the AR and morphology (Fig. 3a). TEM sizing of a mixture exhibited broader AR distribution due to overlapping peaks at 4.0 and 5.4. The 1.5 – 2.0 AR peaks were from the small presence of synthesis byproducts (spheres, cubes, and stars). Spectral overlap of nanocapsules and nanobones at both excitation wavelengths was minimal (Fig. 3b, black).

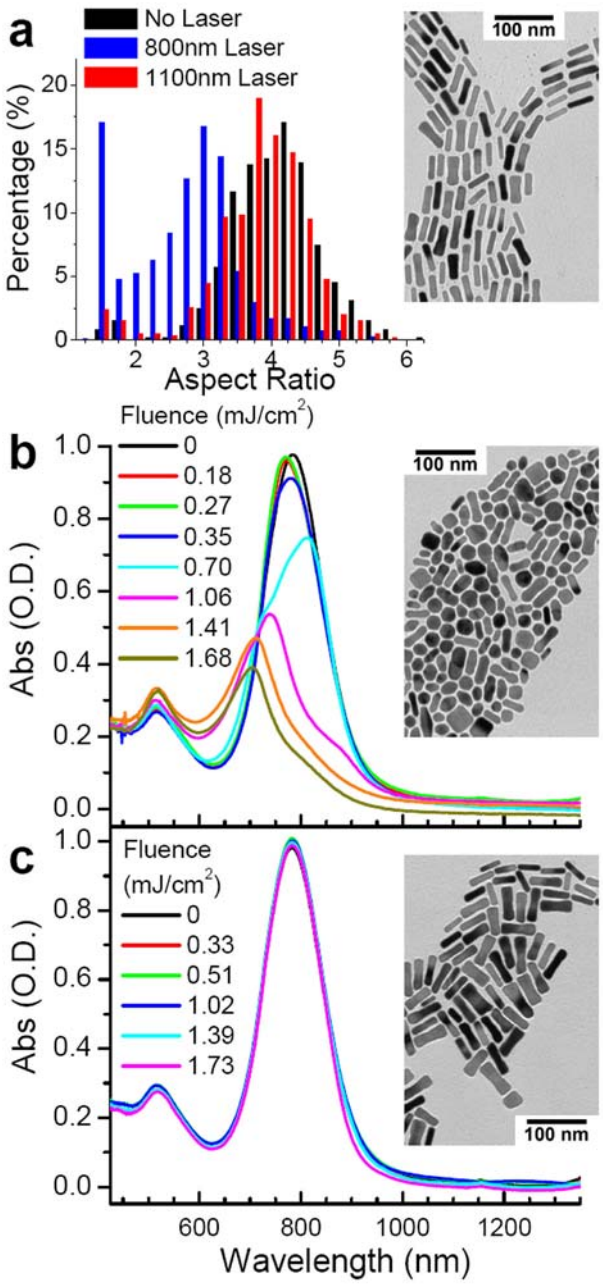

Figure 1. Melting nanocapsules. a) AR histogram of nanocapsules exposed to irradiation at 800 nm at 1.68 mJ/cm^2 (blue) and 1100 nm at 1.73 mJ/cm^2 (red), and unexposed (black). TEM image of unexposed nanocapsules sample (inset). b) optical absorption spectra of nanocapsules upon exposure to λ_{800} irradiation. Fluence (mJ/cm^2): 0 (black), 0.18 (red), 0.27 (green), 0.35 (blue), 0.70 (cyan), 1.06 (pink), 1.41 (orange), 1.68 (olive). Inset: TEM image of λ_{800} irradiated sample with a fluence of 1.68 mJ/cm^2. c) optical absorption of nanocapsules upon exposure to λ_{1100} irradiation. Fluence (mJ/cm^2): 0

(black), 0.33 (red), 0.51 (green), 1.02 (blue), 1.39 (cyan), pink (1.73). Inset: TEM image of λ_{1100} irradiated sample with a fluence of 1.73 mJ/cm^2.

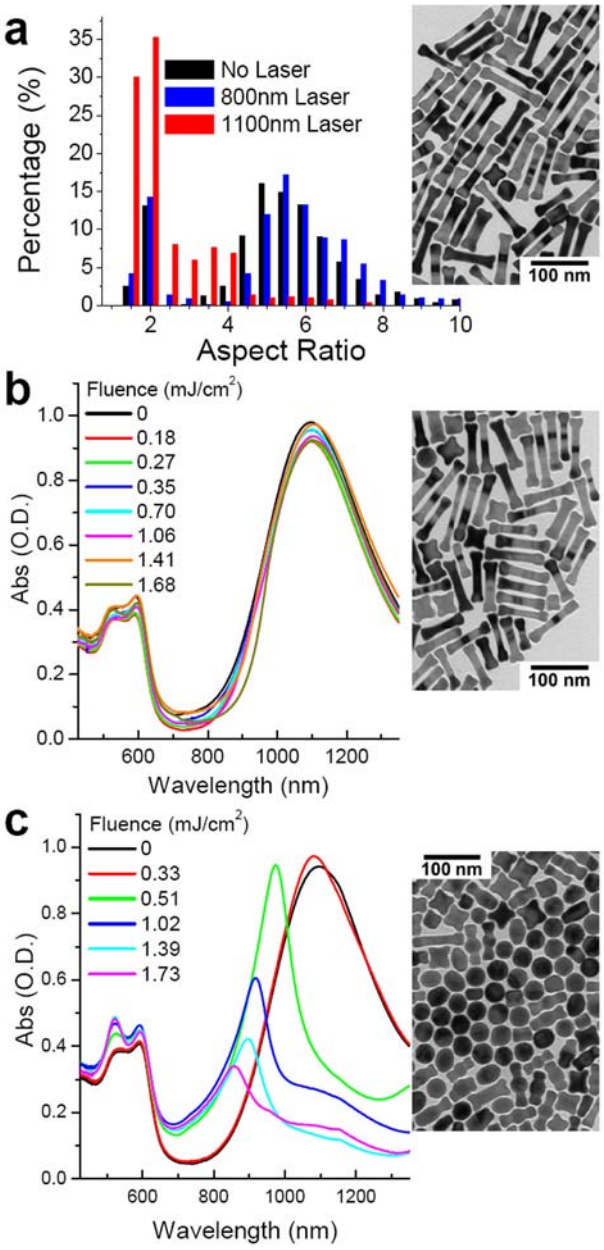

Figure 2. Melting nanobones. a) AR histogram of nanobones exposed to irradiation at 800 nm at 1.68 mJ/cm^2 (blue) and 1100 nm at 1.73 mJ/cm^2 (red), and unexposed (black). TEM image of unexposed nanobones sample (inset). b) optical absorption spectra of nanobones upon exposure to λ_{800} irradiation. Fluence (mJ/cm^2): 0 (black), 0.18 (red), 0.27 (green), 0.35 (blue), 0.70 (cyan), 1.06 (pink), 1.41

(orange), 1.68 (olive). Inset: TEM image of λ_{800} irradiated sample with a fluence of 1.68 mJ/cm^2. c) optical absorption of nanobones upon exposure to λ_{1100} irradiation. Fluence (mJ/cm^2): 0 (black), 0.33 (red), 0.51 (green), 1.02 (blue), 1.39 (cyan), pink (1.73). Inset: TEM image of λ_{1100} irradiated sample with a fluence of 1.73 mJ/cm^2.

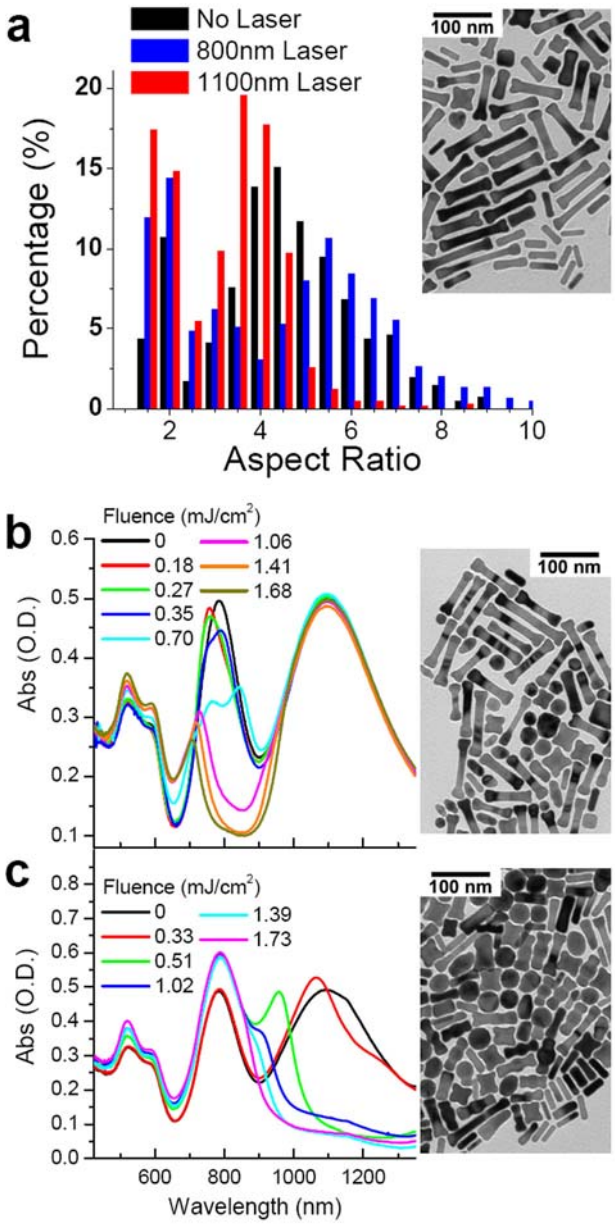

Figure 3. Selective melting of nanocapsule/nanobone mixtures. a) AR histogram of nanocapsules-nanobones mixture exposed to irradiation at 800 nm at 1.68 mJ/cm^2 (blue) and 1100 nm at 1.73 mJ/cm^2

(red), and unexposed (black). Inset: TEM image of unexposed mixture. b) optical absorption spectrum of mixture after λ_{800} irradiation. Fluence (mJ/cm^2): 0 (black), 0.18 (red), 0.27 (green), 0.35 (blue), 0.70 (cyan), 1.06 (pink), 1.41 (orange), 1.68 (olive). Inset: TEM image λ_{800} irradiated mixture with a fluence of 1.68 mJ/cm^2. c) optical absorption spectrum of mixture after λ_{1100} irradiation. Fluence (mJ/cm^2): 0 (black), 0.33 (red), 0.51 (green), 1.02 (blue), 1.39 (cyan), pink (1.73). Inset: TEM image λ_{1100} irradiated mixture with a fluence of 1.73 mJ/cm^2.

Laser irradiation of gold NRs at SPR_{long} caused melting,[18, 19] accompanied by a shape transformation to spheres. We studied the fluence dependence of nanocapsule and nanobone melting by monitoring absorption. λ_{800} irradiation of nanocapsules caused the SPR_{long} to decrease in intensity and blue-shift with increasing fluence, while the ~520 nm peak increased (Fig. 1b). This suggested that melting transformed nanocapsules into shorter rods and spheres. TEM images of nanocapsules after λ_{800} irradiation (inset) and size analysis showed the AR distribution shift to lower values (Fig. 1a, blue), supporting shape transformation to spheres. To show that melting of nanocapsules requires matching irradiation wavelength to the SPR_{long}, we irradiated nanocapsules at 1100 nm. The absorption spectrum was unchanged (Fig. 1c), demonstrating no significant effect. TEMs of nanocapsules after λ_{1100} irradiation (inset) were also unchanged, and size analysis showed little effect on the AR distribution (Fig. 1a, red).

The melting of the nanobones also required the matching of the irradiation wavelength to their SPR_{long}. When nanobones were exposed to λ_{1100} irradiation, the 1100 nm peak decreased and blue-shifted with increasing fluence, while the ~520 nm peak increased (Fig. 2c). TEM imaging after λ_{1100} irradiation confirmed a shape transformation into shorter “candy-wrap” or ϕ-shaped particles and spheres (inset).[25] Size analysis confirmed an AR shift to lower values (Fig. 2a, red). λ_{800} irradiation had essentially no effect, as evidenced by no significant change in absorption scans (Fig. 2b). TEM after λ_{800}

irradiation (inset) and size analysis showed no significant changes in the AR distribution (Fig. 2a, blue), indicating no shape transformation occurred.

We also selectively melted either the nanocapsules or nanobones when both were present in a mixture. The absorption scan had peaks at 800 and 1100 nm due to the presence of both species, and TEMs and AR histograms showed both populations (Fig. 3a, black and inset). λ_{800} irradiation caused the 800 nm peak to decrease, leaving the 1100 nm peak relatively unaffected (Fig. 3b). After λ_{800} irradiation, fewer nanocapsules were present relative to nanobones. Spheres appeared, resulting from the nanocapsule shape transformation (inset). The AR peak at 4.0 decreased in intensity, and peaks at 3.0 or less increased, suggesting melting to form spheres and shorter NRs (Fig. 3a, blue). However, the peak at 5.4 was relatively unchanged. These results support that λ_{800} irradiation melted only the nanocapsules but not the nanobones. When the mixture was exposed to λ_{1100} irradiation, the 1100 nm peak decreased with increasing fluence (Fig. 3c) while the 800 nm peak increased, presumably due to shape transformation of nanobones into ϕ-shaped NRs, which are expected to absorb at wavelengths lower than 1100 nm.[25] TEM imaging after λ_{1100} irradiation (inset) showed that the nanobones disappeared, with primarily nanocapsules, spheres, and ϕ–shaped NRs remaining. The AR peak at 5.4 decreased while peaks at 4.0 or less increased, indicating nanobone shape transformation (Fig. 3a, red). Evidently, λ_{1100} irradiation affected only the nanobones and not nanocapsules. Thus, laser irradiation could selectively melt each species in a mixture, corroborating single-type NRs melting studies.

NRs were conjugated to thiolated DNA 40mers, which were each labeled with different fluorophores and thus distinguishable. Ligand exchange was necessary to avoid aggregation during DNA conjugation, and was performed prior to conjugation to replace the positively charged CTAB surfactant with negatively charged mercaptohexanoic acid.[26] The conjugations were done via charge screening methods.[26-28] Gel electrophoresis assayed DNA conjugation (Fig. 4a-b). Nanocapsules ran toward the positive electrode, indicating a negative charge from the mercaptohexanoic acid ligand coating the surface (Lane 1). Nanocapsules incubated with thiolated 6-carboxyfluorescein-labeled DNA 40mers

(FAM-DNA-SH) were retarded, indicating a larger hydrodynamic radius due to conjugation (Lane 2). The UV image of the gel (Fig. 4b) showed that the free FAM-DNA-SH band after conjugation (Lane 2) was dimmer than the equal-concentration free FAM-DNA-SH alone (Lane 3), also supporting conjugation to nanocapsules, which quench fluorescence. Nanobones showed similar results for thiolated tetramethylrhodamine-labeled DNA 40mers (TMR-DNA-SH). The TMR-DNA-nanobones band (Lane 5) was retarded compared to nanobones alone (Lane 4), and the free TMR-DNA-SH band (Lane 5) was dimmer than the equal-concentration free TMR-DNA-SH alone (Lane 6). These results confirm DNA conjugation to both species. DNA loading on the NR surface was quantified by two methods. The fluorescence change of the supernatant with and without NRs measured the loss of free DNA that was due to NR conjugation. In addition, purified NRs conjugated to DNA were treated with high concentrations mercaptohexanol (MCH), which displaced conjugated DNA from the NR surface. This displaced DNA was quantified by fluorescence. Both methods gave similar estimates of the DNA loadings, which was approximately 114 DNA/nanocapsule and 284 DNA/nanobone.[26, 29-31]

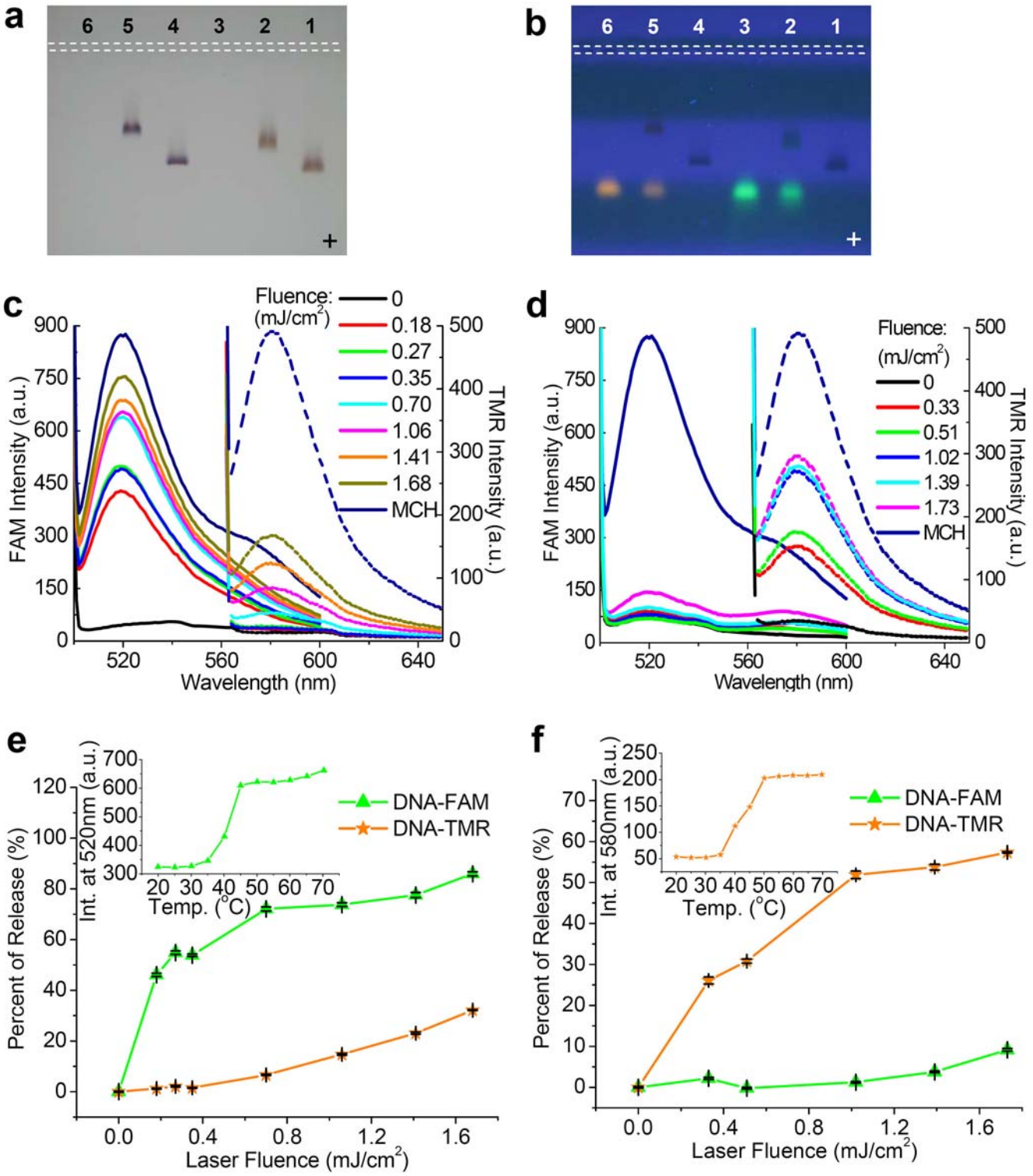

Figure 4. DNA functionalization of NRs and selective release. a) white light and b) UV images of gel electrophoresis. Lane 1: nanocapsules, 2: FAM-DNA-SH + nanocapsules, 3: FAM-DNA-SH, 4: nanobones, 5: TMR-DNA-SH + nanobones, 6: TMR-DNA-SH. Dashed lines indicate positions of wells. Positive direction indicated. c) Fluorescence spectra of supernatant after λ_{800} irradiation, FAM-DNA

peaks (solid lines) and TMR-DNA peaks (dashed lines). Fluence (mJ/cm^2): 0 (black), 0.18 (red), 0.27 (green), 0.35 (blue), 0.70 (cyan), 1.06 (pink), 1.41 (orange), 1.68 (olive). d) fluorescence spectra of supernatant after λ_{1100} irradiation. FAM-DNA peaks (solid lines) and TMR-DNA peaks (dashed lines). Fluence (mJ/cm^2): 0 (black), 0.33 (red), 0.51 (green), 1.02 (blue), 1.39 (cyan), pink (1.73). e) % released of FAM-DNA (green triangles) and TMR-DNA (orange stars) as a function of λ_{800} laser fluence. Inset: melting curve of released DNA (after λ_{800} irradiation of 1.68 mJ/cm^2) hybridized with a DABCYL-complement; monitoring fluorescence at 520nm. f) % released of FAM-DNA (green triangles) and TMR-DNA (orange stars) as a function of λ_{1100} laser fluence. Inset: melting curve of released DNA (after λ_{1100} irradiation of 1.73 mJ/cm^2) hybridized with a DABCYL-complement; monitoring fluorescence at 580 nm. Error bars represent standard deviation from 10 measurements.

Finally, the mixture of purified FAM-DNA-nanocapsules and TMR-DNA-nanobones was laser irradiated for selective release (Scheme 1). Exposure to laser irradiation was followed immediately by centrifugation, and released DNA in the supernatant was quantified by fluorescence spectroscopy. After λ_{800} irradiation, the supernatant fluorescence at 520 nm increased with fluence (Fig. 4c, solid lines), illustrating FAM-DNA release. However, increased fluorescence at 580 nm was much lower, indicating insignificant TMR-DNA release (dashed lines). Therefore, λ_{800} irradiation could selectively release FAM-DNA from nanocapsules, while leaving TMR-DNA-nanobones undisturbed. At fluences <1.00 mJ/cm^2, FAM-DNA release was selective, reaching ~70 % while TMR-DNA release was ≤ 10 %, where 100% was the amount released by MCH treatment (Fig. 4e). For fluences > 1.00 mJ/cm^2, release of TMR-DNA from nanobones did increase, while FAM-DNA release was saturated. When the mixture was exposed to λ_{1100} irradiation, supernatant fluorescence at 580 nm increased (Fig. 4d, dashed lines), while intensity at 520 nm was negligible (solid lines), illustrating TMR-DNA release with no significant FAM-DNA release. TMR-DNA release was selective, reaching 50 – 60% while FAM-DNA release was

< 10% (Fig. 4f). Therefore, λ_{1100} irradiation could selectively release TMR-DNA from nanobones, while leaving FAM-DNA-nanocapsules undisturbed. Evidently, the NRs undergo a shape transformation at these fluences (Figs. 1- 3), which probably induces release due to gold-thiol bond dissociation.[32, 33] We observed that re-adsorption of the released DNA back onto the melted gold nanorods after a long period of time (3 months) was minimal (Fig. S1, Supporting Information). We also observed that the laser irradiation had no effect on the fluorescence of the FAM-DNA and TMR-DNA (Fig. S2, Supporting Information).

We confirmed that released DNA was still functional and could hybridize to a complement. Released DNA was incubated with DABCYL-functionalized DNA complements, and hybrid formation confirmed by melting curves. Dequenching of FAM at 520 nm (Fig. 4e, inset) and TMR at 585 nm (Fig. 4f inset) was monitored with increasing temperature. Both curves were characteristic of functional hybrids, with T_m's coinciding with that of the plain DNA (T_m = 42 °C).

In conclusion, we demonstrate selective release of two distinct DNA oligonucleotides from two different NRs via selective laser-induced melting of NRs. Because laser fluence governs the degree of NR melting, yield and specificity of DNA release, the controlled releases are externally tunable. Tuning NR synthesis parameters could extend this approach beyond two species. Since conjugation requires only standard thiol conjugation, it is potentially applicable to a wide range of molecules. NRs have relatively large surface area and the capacity to loads hundreds of molecules, and ~80% of the payload can be released. NRs are chemically versatile, with customizable coatings, and others have demonstrated active targeting by decorating the NRs with moieties such as antibodies and cell receptor ligands. Others have also utilized laser-induced melting of a single type of NR for controlled release inside cells, while maintaining cell viability by tuning the laser parameters appropriately.[19] Therefore, this proof of concept triggered release from NRs is potentially a powerful technique for improving drug delivery strategies.

METHODS

GOLD NANOROD SYNTHESIS

Both nanocapsules and nanobones were synthesized using the seed-mediated growth method. The preparation of the seed solution was the same for both. Typical protocol: 7.5 ml of 0.2 M CTAB solution was mixed with 0.25ml 0.01M $HAuCl_4$ (for nanocapsules) or 2.5 ml 0.001 M $HAuCl_4$ (for nanobones) in a beaker. While the solution was vigorously stirred, 0.6 ml of ice-cold 0.01 M of $NaBH_4$ was added and the solution turned brownish yellow. Vigorous stirring continued for another 2 min and then it was kept undisturbed at room temperature.

Nanocapsules were synthesized by single-surfactant seed-mediated growth method.[23] Typical protocol for growing nanocapsules: 10 ml of 0.01 M of $HAuCl_4$ was added into 237.5 ml 0.1 M CTAB in a glass bottle, and the solution turned orange. 1.5 ml of 0.01 M $AgNO_3$ was added to the solution, followed by gentle mixing. 1.6 ml of 0.1 M ascorbic acid was added into the solution, followed by gentle inversion until the solution turned colorless. 2 ml of seed solution was gently added to the growth solution. The solution sat on the bench undisturbed overnight, during which it turned reddish brown.

Nanobones were synthesized by binary surfactant seed-mediated growth method.[21, 22] Typical protocol: 125 ml of 0.001 M of $HAuCl_4$ was added into a mixture of 50 ml of 0.3 M CTAB and 75 ml of 0.3 M of BDAC (benzyldimethylhexadecylammonium chloride) in a glass bottle, and the solution turned orange. 5 ml of 0.004 M $AgNO_3$ was added to the solution, followed by gentle mixing. 1.5 ml of 0.1 M ascorbic acid was then added into the solution, followed by gentle inversion until the solution turned colorless. 0.25 ml of seed solution was gently added to the growth solution. The solution sat on the bench undisturbed overnight, during which it turned reddish purple. The resulting product was high aspect ratio gold nanorods. In order to turn these nanorods to nanobones, 4.63 ml of 0.1 M ascorbic acid was added into 250 ml of the nanorod solution, followed by gentle mixing. Reactions were left undisturbed at room temperature. After ~3 hrs the solution turned blue, indicating formation of nanobones.

NANOROD CHARACTERIZATION

Nanorod concentrations were quantified by optical absorption using estimated extinction coefficients.[30] Cary 500 UV-VIS-NIR Spectrophotometer (Varian Inc.) was used to scan the absorption profiles of NRs solutions. Based on their SPR_{long}, we estimated the extinction coefficients to be 4.6 x 10^9 M^{-1} cm^{-1} and 8.6 x 10^9 M^{-1} cm^{-1} for nanocapsules and nanobones respectively. TEM imaging was done on a JEOL 2010 using holey carbon grids. Size analysis was done utilizing ImageJ.[24]

LIGAND EXCHANGE OF NANORODS

The CTAB surfactant on the NR surface was replaced with mercaptohexanoic acid (MHA) by round-trip phase transfer ligand exchange as described in detail in previous work.[26] First we performed aqueous-to-organic phase transfer. Concentrated NR with CTAB surfactants (NR-CTAB) in water was put into contact with dodecanethiol (DDT). After addition of acetone, NRs were extracted into DDT by swirling the solution for a few seconds, upon which the aqueous phase became clear, indicating that no NRs remained. Next, organic-to-aqueous phase transfer was performed. To remove the excess DDT, the DDT coated NRs (NR-DDT) was diluted in toluene. Centrifugation was performed to collect the NR-DDT. Methanol may be needed to precipitate the NR-DDT prior to centrifugation. The collected NR-DDT was resuspended in 1 of mL toluene by brief sonication. The NR-DDT in toluene was then added to 9 mL of 0.01 M mercaptohexanoic acid (MHA) in toluene at 95 °C and vigorously stirred. Reflux and stirring continued until visible aggregation was observed (within ~15 min), and then the solution was allowed to settle and cool to room temperature. Aggregation indicated that NRs were successfully coated by MHA, which are insoluble in toluene. The aggregates were washed 2× with toluene via decantation and then once with isopropanol to deprotonate the carboxylic acid. The aggregates spontaneously redispersed in 1× tris-borate-EDTA buffer (TBE) and were no longer soluble in toluene. This ligand exchange protocol was performed for both types of NR (nanocapsules and nanobones).

DNA FUNCTIONALIZATION OF NANORODS

40mers DNA oligonucleotides with sequences 5’ HS-TTTTT TTTTT TTTTT TTTTT TTTTT TCGGC CCGTA TAATT 3’, fluorescently labeled at the 3’ ends with either 6-carboxyfluorescein (FAM-DNA-SH) or tetramethylrhodamine (TMR-DNA-SH), were purchased from Sigma Aldrich. DNA conjugation was achieved following charge screening protocols.[26-28] Charge screening (salt-aging) was necessary to compensate for electrostatic repulsion between the negatively charged ligand exchanged nanorods and DNA. Sodium dodecyl sulfate (SDS) surfactant was used to increase the stability of nanorods during the salt-aging process. First, FAM-DNA-SH and TMR-DNA-SH were reduced by tris[2-carboxyethyl] phosphine (TCEP) with TCEP:DNA ratio of 100:1. Then nanocapsules or nanobones in the concentration range of 5-10 nM were incubated with the reduced FAM-DNA-SH or TMR-DNA-SH, respectively, in 10 mM phosphate buffer with 0.3% SDS concentration. DNA to NR ratios were 200 FAM-DNA-SH/nanocapsule and 400 TMR-DNA-SH/nanobone. After 3 hrs of incubation, charge screening was performed with salting buffer of 0.6 M of NaCl, 0.3 % SDS in 10 mM phosphate buffer. 8 μL of the salting buffer were added to the 200 μl of the conjugation solution every 30 min followed by 10 s sonication. This step was repeated for total 5 times, which was then followed by overnight incubation.

Two methods were used to confirm NR-DNA conjugation. First, gel electrophoresis was used to observe mobility changes to assay any change in the hydrodynamic radius of DNA-conjugated NRs. Gel electrophoresis was performed with 0.5 % agarose gels in 0.5× TBE. Glycerol was used for loading the samples to ensure the nanorods stayed in the wells prior to traveling in the gel matrix.

The second method to confirm the conjugation was quantification of the DNA loading onto the NR surface. This was accomplished by two methods. First, we quantified the free unconjugated DNA via fluorescence spectroscopy of the fluorophore labels (FAM for nanocapsules and TMR for nanobones) with or without nanorods present. This was done by collecting the supernatants after centrifugation of the conjugation solution. The second method was accomplished by chemical displacement of the conjugated DNA using literature methods.[26, 31] Briefly, purified NR-DNA conjugates were incubated in

1 mM mercaptohexanol (MCH) overnight; displacing the DNA from the NRs. Free displaced DNA was separated from the NRs by centrifugation and quantified by fluorescence spectroscopy. Both methods gave similar estimates of the DNA loadings of approximately 114 DNA/nanocapsule and 284 DNA/nanobone. [30]

LASER IRRADIATION

Laser irradiation was achieved using pulsed femtosecond lasers. For the 800 nm irradiation, the 82 MHz output of a Ti:sapphire oscillator (Tsunami, Spectra-Physics) is amplified at 1 kHz by a Ti:sapphire regenerative amplifier (Spitfire, Spectra-Physics) pumped by the doubled output of a Q-switched Nd:YLF laser (Empower, Spectra-Physics). The system produces 50 - 475 μJ, with duration of 100 fs centered at ~800 nm at a 1 kHz repetition rate. Spot size was 6 mm. Two filter lenses (900 nm shortpass and 700 nm longpass) were placed prior to the sample holder. In a typical experiment, 50 μL of sample in 3x3mm quartz cuvette was exposed to laser for 60 s.

The 1100 nm was generated via a homebuilt two-stage BBO/$KNbO_3$ optical parametric amplifier pumped with the output of a Ti:Sapphire multipass amplifier (Femtolasers: 30 fs, 1 kHz, 800nm). Although the OPA is optimized for the production of 3μm light, ~2.6 – 13.6 μJ pulses of 1100nm light were generated, the difference frequency between 800 nm and 3 μm, is generated by the OPA and used for the experiments. The generated ~1100nm has duration of 45 fs/pulse with repetition rate of 1 kHz. Spot size was 1 mm. 900 nm longpass filter lens was placed prior to the sample holder. In typical experiments, 50 μL of sample in 3×3 mm quartz cuvette were continuously mixed with pipette tip while being exposed to laser for 60 s.

In the NR melting study we had three samples: nanocapsules, nanobones, and a mixture of both. They were all suspended in a 10 mM CTAB solution. The concentration of nanocapsules sample was ~0.8 nM. The concentration of the nanobones sample was ~0.4 nM. The concentrations of the mixture were ~0.4 nM and ~0.2 nM for the nanocapsules and nanobones respectively. After 800 nm or 1100 nm laser

exposure, samples were diluted with 150 μL of a 10 mM CTAB solution. UV-vis-NIR absorption scans were performed for monitoring their shape transformations.

In the DNA release study, we used a mixture of FAM-DNA-nanocapsules and TMR-DNA-nanobones with concentrations of ~0.4 nM and ~0.2 nM, respectively, in 1× TBE. Samples were washed ≥ 3× with 1× TBE to remove free DNA prior to mixing. After 800 nm or 1100 nm laser exposure, samples were immediately diluted with 150 μL of 1× TBE and followed by centrifugation at 16,100 g for 5 min to remove the NRs and collect the supernatants. Fluorescence spectroscopy was used to quantify the released DNA in supernatants. We quantified the fluorescence intensity of FAM due to FAM-DNA released from nanocapsule and TMR due to TMR-DNA released from nanobones.

To ensure that the released DNA from both nanocapsules and nanobones were still functional, we hybridized them with their complement. The complement was functionalized with a 5' DABCYL (5' DABCYL-AATTATACGGGCCG 3') to quench the FAM and TMR in the hybridized state. Melting curves were obtained in a temperature controlled Peltier module of the fluorescence spectrometer, where the increase of fluorescence of either FAM or TMR was monitored as a function of increasing temperature.

Acknowledgement. We gratefully thank A. Tokmakoff, L. DeFlores, K. Jones, S. Roberts, K. Ramasesha, Z. Ganim, R. Nicodemus, and P. Petersen for use and assistance of their lasers. We thank CMSE for use of their experimental facilities. All work was done at MIT and SBS, IP were funded by the NSF REU program (DBI-0649152).

Supporting Information Available: Additional supporting figures of the DNA release study. This material is available free of charge via the internet at http://pubs.acs.org.

REFERENCES

1. Kremsner, P. G.; Krishna, S., Antimalarial Combinations. *Lancet* **2004,** 364, 285-294.
2. Sengupta, S.; Eavarone, D.; Capila, I.; Zhao, G.; Watson, N.; Kiziltepe, T.; Sasisekharan, R., Temporal Targeting of Tumour Cells and Neovasculature with a Nanoscale Delivery System. *Nature* **2005,** 436, 568-572.
3. Hammer, S. M.; Katzenstein, D. A.; Hughes, M. D.; Gundacker, H.; Schooley, R. T.; Haubrich, R. H.; Henry, W. K.; Lederman, M. M.; Phair, J. P.; Niu, M., *et al.*, A Trial Comparing Nucleoside Monotherapy with Combination Therapy in Hiv-Infected Adults with Cd4 Cell Counts from 200 to 500 Per Cubic Millimeter. *N. Engl. J. Med.* **1996,** 335, 1081-1090.
4. Jain, R. K., The Next Frontier of Molecular Medicine: Delivery of Therapeutics. *Nat. Med.* **1998,** 4, 655-657.
5. Richardson, T. P.; Peters, M. C.; Ennett, A. B.; Mooney, D. J., Polymeric System for Dual Growth Factor Delivery. *Nat. Biotechnol.* **2001,** 19, 1029-1034.
6. Grayson, A. C. R.; Choi, I. S.; Tyler, B. M.; Wang, P. P.; Brem, H.; Cima, M. J.; Langer, R., Multi-Pulse Drug Delivery from a Resorbable Polymeric Microchip Device. *Nat. Mater.* **2003,** 2, 767-772.
7. Shawgo, R. S.; Grayson, A. C. R.; Li, Y. W.; Cima, M. J., Biomems for Drug Delivery. *Curr. Opin. Solid St. M.* **2002,** 6, 329-334.
8. Han, G.; Ghosh, P.; Rotello, V. M., Functionalized Gold Nanoparticles for Drug Delivery. *Nanomedicine* **2007,** 2, 113-123.
9. Bergen, J. M.; Von Recum, H. A.; Goodman, T. T.; Massey, A. P.; Pun, S. H., Gold Nanoparticles as a Versatile Platform for Optimizing Physicochemical Parameters for Targeted Drug Delivery. *Macromol. Biosci.* **2006,** 6, 506-516.
10. Jain, T. K.; Reddy, M. K.; Morales, M. A.; Leslie-Pelecky, D. L.; Labhasetwar, V., Biodistribution, Clearance, and Biocompatibility of Iron Oxide Magnetic Nanoparticles in Rats. *Mol. Pharmaceutics* **2008,** 5, 316-327.
11. Berry, C. C.; Curtis, A. S. G., Functionalisation of Magnetic Nanoparticles for Applications in Biomedicine. *J. Phys. D: Appl. Phys.* **2003,** 36, R198-R206.
12. Gobin, A. M.; Lee, M. H.; Halas, N. J.; James, W. D.; Drezek, R. A.; West, J. L., Near-Infrared Resonant Nanoshells for Combined Optical Imaging and Photothermal Cancer Therapy. *Nano Lett.* **2007,** 7, 1929-1934.
13. Liao, H. W.; Nehl, C. L.; Hafner, J. H., Biomedical Applications of Plasmon Resonant Metal Nanoparticles. *Nanomedicine* **2006,** 1, 201-208.
14. Pissuwan, D.; Valenzuela, S. M.; Cortie, M. B., Therapeutic Possibilities of Plasmonically Heated Gold Nanoparticles. *Trends Biotechnol.* **2006,** 24, 62-67.
15. Verma, A.; Rotello, V. M., Surface Recognition of Biomacromolecules Using Nanoparticle Receptors. *Chem. Commun.* **2005**, 303-312.
16. Oyelere, A. K.; Chen, P. C.; Huang, X. H.; El-Sayed, I. H.; El-Sayed, M. A., Peptide-Conjugated Gold Nanorods for Nuclear Targeting. *Bioconjugate Chem.* **2007,** 18, 1490-1497.
17. Yu, C.; Varghese, L.; Irudayaraj, J., Surface Modification of Cetyltrimethylammonium Bromide-Capped Gold Nanorods to Make Molecular Probes. *Langmuir* **2007,** 23, 9114-9119.
18. Link, S.; Burda, C.; Nikoobakht, B.; El-Sayed, M. A., Laser-Induced Shape Changes of Colloidal Gold Nanorods Using Femtosecond and Nanosecond Laser Pulses. *J. Phys. Chem. B* **2000,** 104, 6152-6163.
19. Chen, C.-C.; Lin, Y.-P.; Wang, C.-W.; Tzeng, H.-C.; Wu, C.-H.; Chen, Y.-C.; Chen, C.-P.; Chen, L.-C.; Wu, Y.-C., DNA-Gold Nanorod Conjugates for Remote Control of Localized Gene Expression by near Infrared Irradiation. *J. Am. Chem. Soc.* **2006,** 128, 3709-3715.

20. Sershen, S. R.; Mensing, G. A.; Ng, M.; Halas, N. J.; Beebe, D. J.; West, J. L., Independent Optical Control of Microfluidic Valves Formed from Optomechanically Responsive Nanocomposite Hydrogels. *Adv. Mater.* **2005,** 17, 1366-1368.
21. Gou, L. F.; Murphy, C. J., Fine-Tuning the Shape of Gold Nanorods. *Chem. Mater.* **2005,** 17, 3668-3672.
22. Nikoobakht, B.; El-Sayed, M. A., Preparation and Growth Mechanism of Gold Nanorods (Nrs) Using Seed-Mediated Growth Method. *Chem. Mater.* **2003,** 15, 1957-1962.
23. Sau, T. K.; Murphy, C. J., Seeded High Yield Synthesis of Short Au Nanorods in Aqueous Solution. *Langmuir* **2004,** 20, 6414-6420.
24. Abramoff, M. D.; Magelhaes, P. J.; Ram, S. J., Image Processing with ImageJ. *Biophotonics Intl.* **2004,** 11, 36-42.
25. Horiguchi, Y., Honda K., Kato Y., Nakashima N., Niidome Y., Photothermal Reshaping of Gold Nanorods Depends on the Passivating Layers of the Nanorod Surfaces. *Langmuir* **2008,** 24, 12026-12031.
26. Wijaya, A.; Hamad-Schifferli, K., Ligand Customization and DNA Functionalization of Gold Nanorods Via Roundtrip Phase Transfer Ligand Exchange. *Langmuir* **2008,** 24, 9966 - 9969.
27. Hurst, S. J.; Lytton-Jean, A. K. R.; Mirkin, C. A., Maximizing DNA Loading on a Range of Gold Nanoparticle Sizes. *Anal. Chem.* **2006,** 78, 8313-8318.
28. Zhang, J.; Song, S. P.; Wang, L. H.; Pan, D.; Fan, C., A Gold Nanoparticle-Based Chronocoulometric DNA Sensor for Amplified Detection of DNA. *Nat. Protoc.* **2007,** 2, 2888-2895.
29. Demers, L. M.; Mirkin, C. A.; Mucic, R. C.; Robert A. Reynolds, I.; Letsinger, R. L.; Elghanian, R.; Viswanadham, G., A Fluorescence-Based Method for Determining the Surface Coverage and Hybridization Efficiency of Thiol-Capped Oligonucleotides Bound to Gold Thin Films and Nanoparticles. *Anal. Chem.* **2000,** 72, 5535-5541.
30. Orendorff, C. J.; Murphy, C. J., Quantitation of Metal Content in the Silver-Assisted Growth of Gold Nanorods. *J. Phys. Chem. B* **2006,** 110, 3990-3994.
31. Park, S.; Brown, K. A.; Hamad-Schifferli, K., Changes in Oligonucleotide Conformation on Nanoparticle Surfaces by Modification with Mercaptohexanol. *Nano Lett.* **2004,** 4, 1925-1929.
32. Herdt, A. R.; Drawz, S. M.; Kang, Y.; Taton, T. A., DNA Dissociation and Degradation at Gold Nanoparticle Surfaces. *Colloids Surf., B* **2006,** 51, 130-139.
33. Jain, P. K.; Qian, W.; El-Sayed, M. A., Ultrafast Cooling of Photoexcited Electrons in Gold Nanoparticle-Thiolated DNA Conjugates Involves the Dissociation of the Gold-Thiol Bond. *J. Am. Chem. Soc.* **2006,** 128, 2426-2433.

SYNOPSIS TOC.